Estradiol and mTORC2 cooperate to enhance prostaglandin biosynthesis and tumorigenesis in TSC2-deficient LAM cells

Estradiol and mTORC2 cooperate to enhance prostaglandin biosynthesis and tumorigenesis in TSC2-deficient LAM cells

Chenggang Li,[1] Po-Shun Lee,[2] Yang Sun,[1] Xiaoxiao Gu,[3] Erik Zhang,[1] Yanan Guo,[2] Chin-Lee Wu,[4] Neil Auricchio,[2] Carmen Priolo,[1] Jing Li,[3] Alfredo Csibi,[3,5] Andrey Parkhitko,[1] Tasha Morrison,[1] Anna Planaguma,[1] Shamsah Kazani,[1] Elliot Israel,[1] Kai-Feng Xu,[6] Elizabeth Petri Henske,[1] John Blenis,[3] Bruce D. Levy,[1] David Kwiatkowski,[2] and Jane J. Yu[1]

[1]Pulmonary and Critical Care Medicine, [2]Translational Medicine, Department of Medicine, Brigham and Women's Hospital-Harvard Medical School, Boston, MA 02115
[3]Department of Cell Biology, Harvard Medical School, Boston, MA 02115
[4]Massachusetts General Hospital, Boston, MA 02115
[5]Infinity Pharmaceuticals, Inc., Cambridge, MA 02139
[6]Peking Union Medical College, Beijing 100730, China

Lymphangioleiomyomatosis (LAM) is a progressive neoplastic disorder that leads to lung destruction and respiratory failure primarily in women. LAM is typically caused by *tuberous sclerosis complex 2* (*TSC2*) mutations resulting in mTORC1 activation in proliferative smooth muscle–like cells in the lung. The female predominance of LAM suggests that estradiol contributes to disease development. Metabolomic profiling identified an estradiol-enhanced prostaglandin biosynthesis signature in Tsc2-deficient (TSC^{-}) cells, both in vitro and in vivo. Estradiol increased the expression of cyclooxygenase-2 (COX-2), a rate-limiting enzyme in prostaglandin biosynthesis, which was also increased at baseline in TSC-deficient cells and was not affected by rapamycin treatment. However, both Torin 1 treatment and Rictor knockdown led to reduced COX-2 expression and phospho-Akt-S473. Prostaglandin production was also increased in TSC-deficient cells. In preclinical models, both Celecoxib and aspirin reduced tumor development. LAM patients had significantly higher serum prostaglandin levels than healthy women. 15-epi-lipoxin-A_4 was identified in exhaled breath condensate from LAM subjects and was increased by aspirin treatment, indicative of functional COX-2 expression in the LAM airway. In vitro, 15-epi-lipoxin-A_4 reduced the proliferation of LAM patient–derived cells in a dose-dependent manner. Targeting COX-2 and prostaglandin pathways may have therapeutic value in LAM and TSC-related diseases, and possibly in other conditions associated with mTOR hyperactivation.

CORRESPONDENCE
Jane Yu:
jyu13@partners.org
OR
David Kwiatkowski:
dkwiatkowski@
rics.bwh.harvard.edu

Abbreviations used: EBC, exhaled breath condensate; ELT3, Tsc2-deficient rat uterus–derived cells; LAM, lymphangioleiomyomatosis; MILES, multicenter international LAM efficacy of sirolimus; shRNA, short hairpin RNA; TSC, tuberous sclerosis complex.

Lymphangioleiomyomatosis (LAM) is a progressive pulmonary disease which affects almost exclusively women. LAM is characterized pathologically by widespread proliferation of abnormal smooth muscle cells, which typically have the *tuberous sclerosis complex 2* (*TSC2*) mutation leading to mTORC1 activation, and by cystic changes within the lung parenchyma (McCormack et al., 2010, 2012; Taveira-DaSilva et al., 2010; Henske and McCormack, 2012; Krymskaya, 2012). LAM occurs in 30–40% of women with TSC (Costello et al., 2000; Dabora et al., 2001). However, LAM is more commonly diagnosed in women who do not have clinical features of TSC or germline mutations in *TSC1* or *TSC2* (sporadic LAM). Inactivating mutations of both alleles of the *TSC1* or *TSC2* have been found in LAM cells from both TSC-LAM and sporadic LAM patients (Astrinidis et al., 2000; Strizheva et al., 2001).

Approximately 60% of women with the sporadic form of LAM also have renal angiomyolipomas (Ryu et al., 2012). The presence of

C. Li, P.-S. Lee, and Y. Sun contributed equally to this paper.

The Rockefeller University Press $30.00
J. Exp. Med. 2014 Vol. 211 No. 1 15-28
www.jem.org/cgi/doi/10.1084/jem.20131080

The Journal of Experimental Medicine

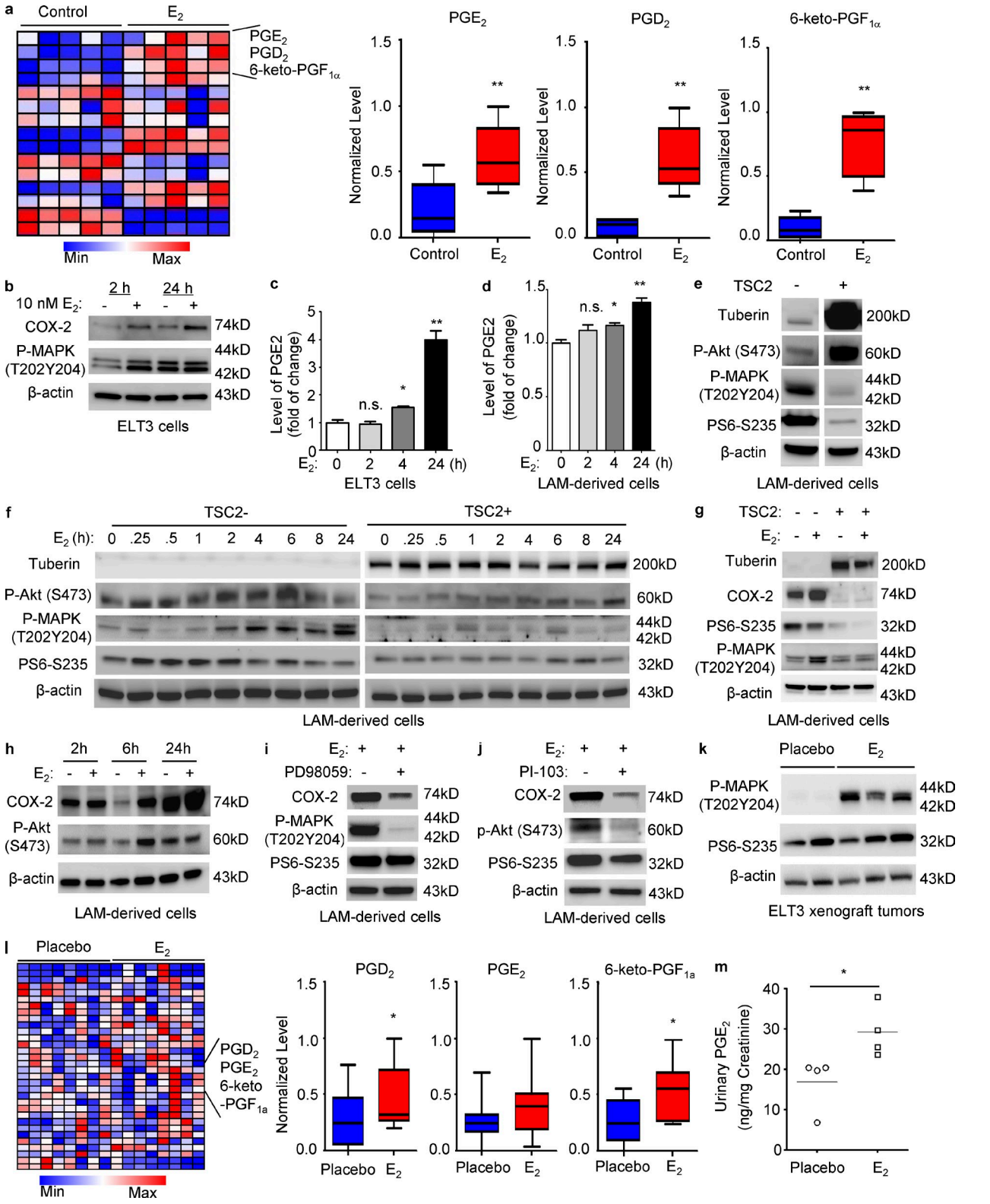

Figure 1. Identification of an estradiol–induced prostaglandin biosynthesis signature in cells and preclinical models. (a) ELT3 cells were treated with 10 nM estradiol for 24 h. Cellular metabolites were profiled by mass spectrometry ($n = 5$; Metabolon LC-MS/MS). Box plots of PGE_2 (6.0–59.6 ng), PGD_2 (1.3–7.2 ng), and 6-keto $PGF_{1\alpha}$ (2.5–18.3 ng) are shown. Data show the mean of five sets of independent samples. **, $P < 0.01$; Welch's *t* tests and Wilcoxon rank sum tests. (b) Immunoblot analysis of ELT3 cells treated with estradiol for 2 or 24 h. β-Actin was used as a loading control. (c and d) Secreted PGE_2 levels were measured in conditioned media collected from cells treated with estradiol or control at the indicated times. Data were normalized to

TSC2 mutations in LAM cells and renal angiomyolipoma cells from women with sporadic LAM, but not in normal tissues, has led to the model that LAM cells spread to the lungs via a metastatic mechanism, despite the fact that LAM cells have a histologically benign appearance (Astrinidis et al., 2000; Karbowniczek et al., 2003; Crino et al., 2006). Genetic and molecular analyses of recurrent LAM after lung transplantation support this benign metastatic model (Karbowniczek et al., 2003).

The protein products of *TSC1* and *TSC2*, hamartin and tuberin, respectively, form a heterodimer (Plank et al., 1998; Jaeschke et al., 2002) that inhibits the small GTPase Rheb (Ras homologue enriched in brain), via tuberin's highly conserved GTPase-activating protein domain. Loss of tuberin or hamartin leads to hyperactivation of the mammalian target of Rapamycin complex 1 (mTORC1), in LAM cells, other TSC tumors, and multiple animal models (Manning, 2010). mTORC1 regulates cell growth, protein translation, and metabolism (Düvel et al., 2010). In a randomized MILES (Multicenter International LAM Efficacy of Sirolimus) trial, the mTORC1 inhibitor rapamycin stabilized lung function and improved symptoms in LAM patients (McCormack et al., 2011). However, lung function declined when rapamycin was discontinued.

The female predominance of LAM strongly suggests that estradiol contributes to disease pathogenesis (Henske and McCormack, 2012; McCormack et al., 2012). We have demonstrated that estradiol treatment increases levels of circulating tumor cells and pulmonary metastases of TSC2-deficient cells in a xenograft model of LAM (Yu et al., 2009). Other studies have demonstrated that estradiol induces COX-2–mediated prostaglandin synthesis (Egan et al., 2004). COX-2 is a rate-limiting enzyme catalyzing the conversion of arachidonate to prostaglandins. COX-2 overexpression has been documented in human tumors, and prostaglandins may contribute to cancer development (FitzGerald and Patrono, 2001; Müller, 2004; Wang et al., 2007; Wang and Dubois, 2010). In this study, we discovered that estradiol enhances prostaglandin production by TSC2-deficient cells. Furthermore, loss of TSC2 increases COX-2 and prostaglandin biosynthesis in a rapamycin-insensitive but Torin 1-sensitive and Rictor-dependent manner, suggesting an mTORC1-independent but mTORC2-dependent mechanism. We also showed that loss of TSC2 leads to alterations in the cellular distribution of EGFR, and this appears to be the mechanism by which it causes increased PG biosynthesis. Celecoxib reduced renal tumor incidence in a spontaneous-arising $Tsc2^{+/-}$ mouse tumor model, and aspirin suppressed tumor progression in a xenograft tumor model. This study indicates that targeting COX-2 with aspirin or related drugs may have therapeutic benefit in LAM and TSC-related diseases.

RESULTS

Identification of an estradiol-induced prostaglandin biosynthesis signature in TSC2-deficient cells in vitro and in vivo

To examine the possible effects of estradiol on metabolic pathways in TSC2-deficient rat uterus–derived (ELT3) cells, we performed a metabolomic screen. A significant increase in prostaglandins including PGE_2, PGD_2, and 6-keto-$PGF_{1\alpha}$, was seen in estradiol-treated cells (Fig. 1 a). Furthermore, estradiol increased p44/42–MAPK T202/Y204 phosphorylation, COX-2 expression, and PGE_2 levels in TSC2-deficient cells at 2 and 24 h (Fig. 1, b and c). Analysis of LAM patient–derived TSC-deficient 621–101 cells (Yu et al., 2004) showed that estradiol also increased PGE_2 levels at 24 h (Fig. 1 d), confirming the results in the TSC2-deficient ELT3 cells.

To define the impact of estradiol on activation of signaling pathways, we first compared the basal levels of phospho-S6, phospho-MAPK, and phospho-Akt S473 for the $TSC2^{+/+}$ and $TSC2^{-/-}$ cells. TSC-deficient cells exhibited lower levels of phospho-Akt S473 and higher levels of phospho-MAPK and phospho-S6, relative to TSC-addbackcells ($TSC2^{+}$; Fig. 1 e). We next performed a time-course analysis of the effect of estradiol on activation of these pathways in both TSC-deficient and TSC-addback LAM-derived cells. We found that estradiol activated Akt S473 within 6 h, MAPK (T202Y204) at 2, 4, 6, 8, and 24 h, but not S6 in TSC2-deficient cells (Fig. 1 f, left). In comparison, estradiol stimulated Akt S473 and MAPK (T202Y204) to a lesser degree in TSC2-addback cells (Fig. 1 f, right). Our data indicate that estradiol activates MAPK and Akt pathways in the absence of TSC2.

To determine whether the effect of estradiol on cells is dependent on TSC defects, we examined the levels of COX-2 using immunoblotting in estradiol-stimulated TSC2-deficient and TSC2-addback cells. Estradiol treatment did not affect COX-2 expression in TSC2-addback LAM patient–derived cells (Fig. 1 g). To address how estradiol exerts its action on COX-2 expression and prostaglandin production, we examined

control group ($n = 3$; ELISA). Results are representative of six sets of independent samples per group from three experiments. (e and f) LAM patient–derived cells were serum-starved for 24 h, and then treated with estradiol for 0.25, 0.5, 2, 4, 6, 8, or 24 h. Immunoblot analyses of tuberin, phospho-Akt S473, phospho-MAPK (T202/Y204), and phospho-S6 (S235/236). (g and h) Immunoblot analyses of COX-2, phospho-S6 (S235/236), phospho-MAPK (T202/Y204), and phospho-Akt S473. (i and j) LAM patient–derived cells treated with 50 µM PD98059 or 5 µM PI-103 for 1 h, and then treated with 10 nM estradiol for 24 h. Immunoblot analyses of COX-2, phospho-S6 (S235/236), phospho-MAPK (T202/Y204), and phospho-Akt S473. (e–j) Results are representative of three different experiments. (k) Levels of phospho-MAPK (Thr202/Tyr204) and phospho-S6 (Ser235/236) from xenograft tumors from placebo or estradiol-treated CB17-scid mice were measured by immunoblotting. (l) Cellular metabolites extracted from xenograft tumors from estradiol or placebo-treated mice were profiled ($n = 8$; Metabolon LC-MS/MS). Box plots of PGE_2 (23.3–133 ng), PGD_2 (6.8–76.96 ng), and 6-keto $PGF_{1\alpha}$ (17.5–167.3 ng) are shown. (k and l) Results are representative of eight mice per group. *, $P < 0.05$; **, $P < 0.01$; Welch's *t* tests and Wilcoxon rank sum tests. (m) Urinary PGE_2 and creatinine from placebo or estradiol-implanted ovariectomized female mice bearing xenograft tumors was measured five-week after cell inoculation (ELISA). PGE_2 levels were normalized to creatinine. Results are representative of four mice per group. *, $P < 0.05$; Student's *t* test.

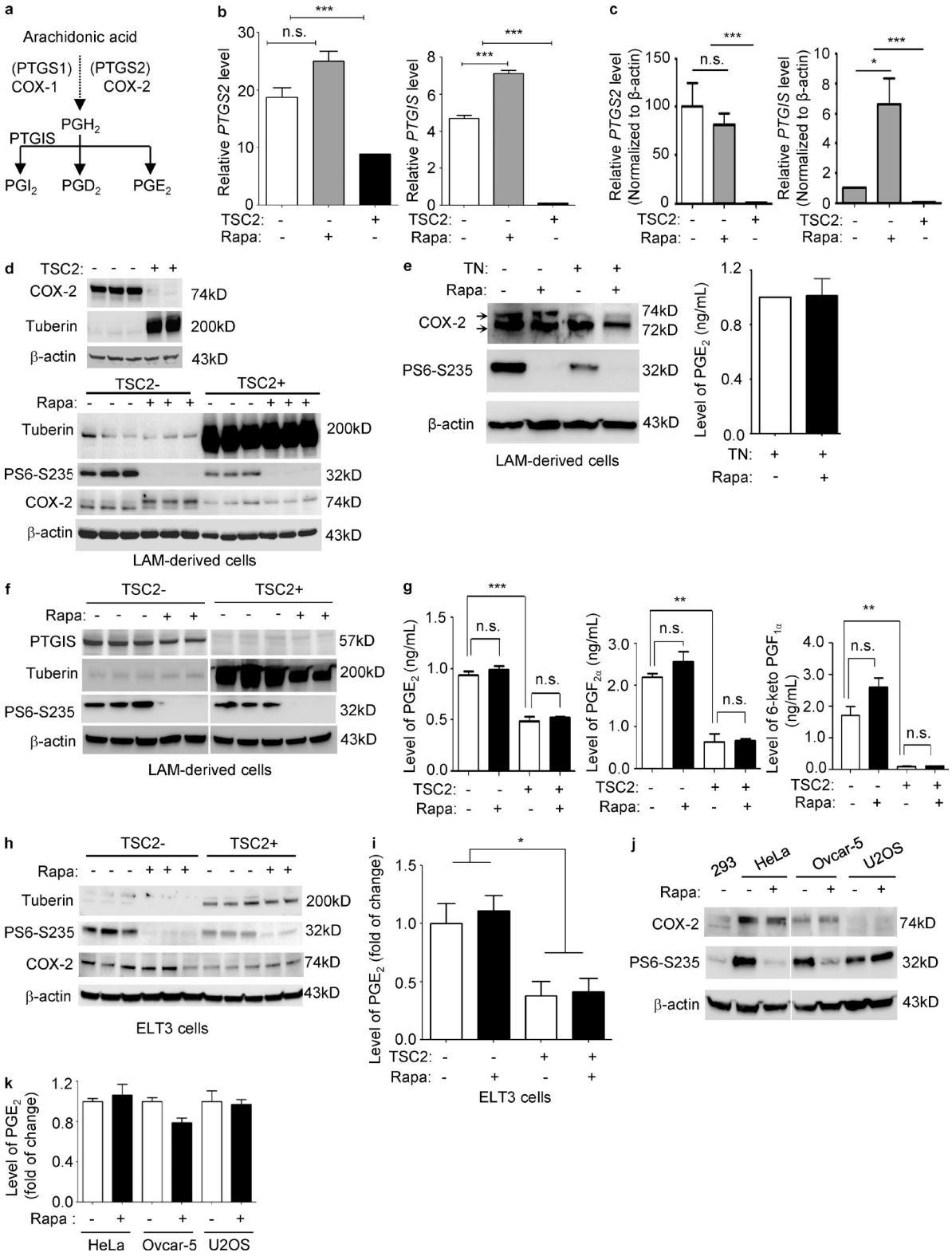

Figure 2. TSC2 negatively regulates COX-2 expression and prostaglandin production in a rapamycin-insensitive but Torin 1 and mTORC2-dependent manner in vitro. (a) Simplified prostaglandin biosynthesis pathway. (b) Re-analysis of previously published expression array data (Lee et al., 2010). Bar graph of the transcript levels of *PTGS2* (COX-2) and *PTGIS* (prostacyclin synthase) in TSC2-deficient (TSC−) and TSCS2-addback (TSC2$^+$) LAM patient-derived cells treated with rapamycin (Rapa) or Vehicle for 24 h. Data show the mean of three sets of independent samples. (c) Real-time RT-PCR analysis of the transcript levels of *PTGS2* and *PTGIS* in TSC2-deficient LAM patient-derived cells relative to TSC2-addback cells treated with 20 nM rapamycin

Table 1. Rapamycin-insensitive up-regulation of *PTGS2* and *PTGIS* expression in TSC-deficient LAM patient-derived cells are not affected by rapamycin treatment compared to TSC2-addback cells

Gene	Protein	Fold change TSC^{-}/vehicle versus TSC2^{+}/vehicle	Fold change TSC2^{-} rapamycin versus TSC2^{-}/vehicle	Fold change TSC2^{-}/rapamycin versus TSC2^{+}/vehicle
PTGS2	COX-2	2.1 (P = 0.004)	1.3 (P = 0.05)	2.8 (P = 0.0006)
PTGIS	Prostacyclin synthase (PGIS)	40.4 (P = 0.00001)	1.5 (P = 0.0006)	61.1 (P = 0.000003)

the activation of p44/42–MAPK and PI3K–Akt, which are known pathways promoting COX-2 expression (Wang and Dubois, 2010). We found that estrogen activates both p44/42–MAPK and PI3K–Akt in TSC2-deficient cells, assessed by phosphorylation at T202/204 and S473 sites, respectively, but not in TSC2-addback cells (Fig. 1, g and h). Inhibition of p44/42–MAPK using PD98059 or PI3K–Akt using PI-103 blocked estrogen-enhanced COX-2 expression (Fig. 1, i and j). Collectively, these data indicate that estradiol activates COX-2 expression via p44/42–MAPK and PI3K–Akt pathways.

To determine the effect of estradiol on cellular metabolism in vivo, we used xenograft tumors of TSC2-deficient ELT3 cells (Yu et al., 2009) from placebo or estradiol-implanted ovariectomized female mice, in which p44/42–MAPK phosphorylation was evident (Fig. 1 k). A metabolomic screen showed that levels of PGE_2, PGD_2, and 6-keto-$PGF_{1\alpha}$ was significantly increased in xenograft tumors from mice treated with estradiol (Fig. 1 l), Estradiol-treated mice bearing ELT3 xenograft tumors also exhibited higher levels of urinary PGE_2 relative to placebo controls (Fig. 1 m). These data demonstrate that estradiol stimulates prostaglandin biosynthesis by TSC2-deficient cells in vitro and in vivo.

TSC2 negatively regulates COX-2 expression and prostaglandin production in vitro and in vivo

Prostaglandins are products of prostaglandin-endoperoxide synthases (PTGSs) 1 and 2, or more commonly known as COX-1 and COX-2 (Fig. 2). COX-1 and COX-2 convert arachidonic acids released from membrane phospholipids into PGH_2. Prostacyclin (PGI_2) is produced by prostacyclin synthase (PTGIS) from PGH_2 (Fig. 2 a). To define the molecular mechanisms responsible for estradiol-enhanced COX-2 expression and prostaglandin production, we analyzed our previous expression array of TSC2-deficient LAM patient–derived cells (Lee et al., 2010) and found that both COX-2 (*PTGS2*) and prostacyclin synthase (*PGTIS)* expression were significantly increased, by 2- and 40-fold, respectively (Fig. 2 b and Table 1), in TSC2-deficient cells relative to TSC2-addback cells. To validate the findings of the expression array, we first performed real-time RT-PCR analysis. TSC2-deficient LAM patient–derived cells exhibited a 102-fold increase of PTGS2, and a 15-fold increase of PTGIS ($P < 0.0001$; Fig. 2 c). Importantly, rapamycin treatment did not affect the levels of PTGS2, but increased the levels of PTGIS by 6.6-fold ($P < 0.05$; Fig. 2 c), consistent with the changes identified in the expression array profile (Lee et al., 2010; Fig. 2 b). We next examined the protein levels of COX-2 and PTGIS using immunoblotting analysis. COX-2 protein levels were higher in TSC2-deficient cells compared with TSC2-addback 621–101 cells (Fig. 2 d). Rapamycin treatment suppressed phosphorylation of the ribosomal protein p70S6 (S6), but did not affect the level of COX-2 expression, although it altered the migration of COX-2 (Fig. 2 d). COX-2 occurs as 72- and 74-kD isoforms, with the larger form a result of glycosylation at Asn580 (Sevigny et al., 2006). LAM cells treated with tunicamycin, an inhibitor of *N*-acetylglucosamine transferases, showed a marked reduction in the slower migrating form of COX-2, but showed similar production of PGE_2 (Fig. 2 e). This implies that this gel shift of COX-2 is caused by increased glycosylation.

Prostacyclin synthase (PTGIS) catalyzes the conversion of PGH_2 to prostacyclin (PGI_2). PTGIS protein levels were markedly higher in TSC2-deficient cells compared with TSC2-addback 621–103 cells (Fig. 2 f). Rapamycin treatment suppressed phosphorylation of the ribosomal protein p70S6 (S6), and decreased PTGIS levels in TSC2-deficient ells to a minor extent, but had no appreciable effect on TSC2-addback cells (Fig. 2 f), suggesting that TSC2 also regulates PTGIS expression independent of mTORC1.

To determine the functional impact of altered expression COX-2 and PGTIS on prostaglandin production, secreted

or vehicle for 24 h. Data show the mean of three sets of independent samples. (d–f) Immunoblot analyses of tuberin, PTGIS, phospho-S6 (S235/236), and COX-2 protein in LAM patient–derived cell treated with 20 nM rapamycin (Rapa), 1 µg/ml tunicamycin (TN), or rapamycin plus tunicamycin, for 24 h. Results are representative of three different experiments. (e and g) Secreted prostaglandin levels were quantified in conditioned media collected from LAM patient–derived cells treated with 20 nM rapamycin (Rapa), 1 µg/ml tunicamycin (TN), or rapamycin plus tunicamycin, for 24 h ($n = 3$; ELISA). Results are representative of three sets of independent samples per group. (h) ELT3 cells were treated with 20 nM rapamycin (Rapa) or control for 24 h. Immunoblot analysis of COX-2 and phospho-S6 (S235/236). Results are representative of three different experiments. (i) Secreted prostaglandin levels were quantified in conditioned media collected from ELT3 cells treated with rapamycin or control. Data were normalized to control group ($n = 3$; ELISA). Results are representative of three sets of independent samples per group. (j) HeLa, OVCAR-5, and U2OS cells were treated with 20 nM rapamycin for 24 h. Immunoblot analysis of COX-2 and phospho-S6 (S235/236). Results are representative of three different experiments. (k) Secreted prostaglandin levels were quantified in conditioned media collected from cells treated with rapamycin or control, data were normalized to control group ($n = 3$; ELISA). Results are representative of three sets of independent samples per group. *, $P < 0.05$; **, $P < 0.01$; ***, $P < 0.005$; Student's *t* test.

levels of PGEM (a stable PGE_2 metabolite), 6-keto-$PGF_{1\alpha}$ (a stable prostacyclin PGI_2 metabolite), and $PGF_{2\alpha}$ were measured from TSC2-deficient LAM patient–derived cells treated with rapamycin or control. Levels of PGE_2, 6-keto-$PGF_{1\alpha}$, and $PGF_{2\alpha}$ were all significantly higher in TSC2-deficient cells relative to TSC2-addback cells, and were also insensitive to rapamycin treatment (Fig. 2 g). Similar results on COX-2 expression were also seen in TSC2-deficient ELT3 cells (Fig. 2 h). PGE_2 levels were elevated by 2.5-fold in ELT3 cells in comparison to TSC2-addback cells, and this again was not affected by rapamycin treatment (Fig. 2 i). To determine whether this phenomenon of rapamycin-insensitive prostaglandin production was seen in other cancer cells with intact TSC2 levels but mTORC1 activation, we examined HeLa, U2OS, and OVCAR5 cells. Although PGE_2 production was variable among these cell lines, rapamycin did not affect COX-2 expression or PGE_2 production, although it did reduce phospho-S6 (Fig. 2, j and k). Together, these data indicate that up-regulation of COX-2 and prostaglandin production is rapamycin-insensitive in cells with mTORC1 activation.

To determine whether TSC2 regulates COX-2 and prostaglandin production in vivo, we used xenograft tumors from mice inoculated with TSC2-deficient ELT3-V3 (vector-control) cells and TSC2-addback ELT3-T3 cells. COX-2 levels were significantly higher in the ELT3-V3 xenograft tumors with elevated phospho-S6 relative to TSC2-addback ELT3-T3 tumors (Fig. 3 a). In addition, levels of PGE_2 in xenograft tumors were significantly higher in mice with the ELT3-V3 tumors in comparison to mice with the TSC2-addback ELT3-T3 tumors (Fig. 3 b). Moreover, urinary PGE_2 level was significantly higher in mice with the ELT3-V3 tumors in comparison to mice with the TSC2-addback ELT3-T3 tumors (Fig. 3 c). Similar results on PGTIS expression were also observed in xenograft tumors of TSC2-deficient ELT3 cells (Fig. 3 d). Urinary 6-keto-PGF1α levels were also significantly higher in mice with the ELT3-V3 tumors in comparison to mice with the TSC2-addback ELT3-T3 tumors (Fig. 3 e). Together, these data indicate that up-regulation of COX-2 and prostaglandin production is rapamycin-insensitive in cells with mTORC1 activation

mTORC2 is a critical mediator of COX-2 expression and prostaglandin biosynthesis in TSC2-deficient cells

To identify additional molecular determinants responsible for rapamycin-insensitive COX-2 expression and prostaglandin biosynthesis, we first treated $Tsc2^{-/-}p53^{-/-}$ MEFs with Torin 1, a potent ATP-competitive mTORC1 and mTORC2 inhibitor for 24 h. Torin 1 decreased the level of COX-2 and phosphorylation of S6 (S235/236) and 4EBP1. Interestingly, cells treated with LY294002, a PI3K inhibitor, for 24 h exhibited reduced level of COX-2. However, rapamycin treatment did not affect the level of COX-2 (Fig. 4 a). Our data suggest that mTORC2 might play a role in mediating COX-2 expression. To further test the impact of mTORC2 on COX-2 expression,

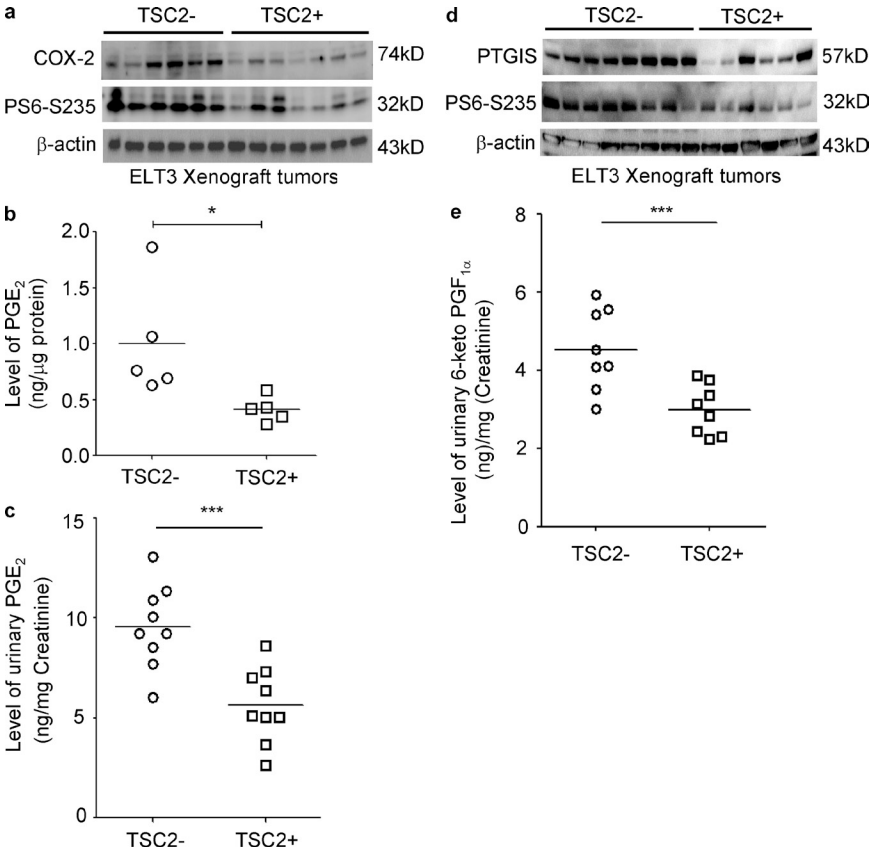

Figure 3. TSC2 negatively regulates COX-2 expression and prostaglandin production in a xenograft tumor model of ELT3 cells. Female CB17-scid mice were inoculated with ELT3-V3 cells (TSC^-, vector addback) or TSC2 addback ($TSC2^+$) ELT3-T3 cells subcutaneously. (a and d) Immunoblot analysis shows levels of phospho-S6 (S235/236), COX-2, and PTGIS in xenograft tumors of ELT3 cells. Levels of PGE_2 in xenograft tumors (b), urinary levels of PGE_2 (c), and 6-keto-$PGF_{1\alpha}$ (e) were normalized to creatinine levels in mice bearing xenograft tumors ($n = 9$; ELISA). Results are representative of five to nine mice per group. *, $P < 0.05$; ***, $P < 0.001$; Student's *t* test.

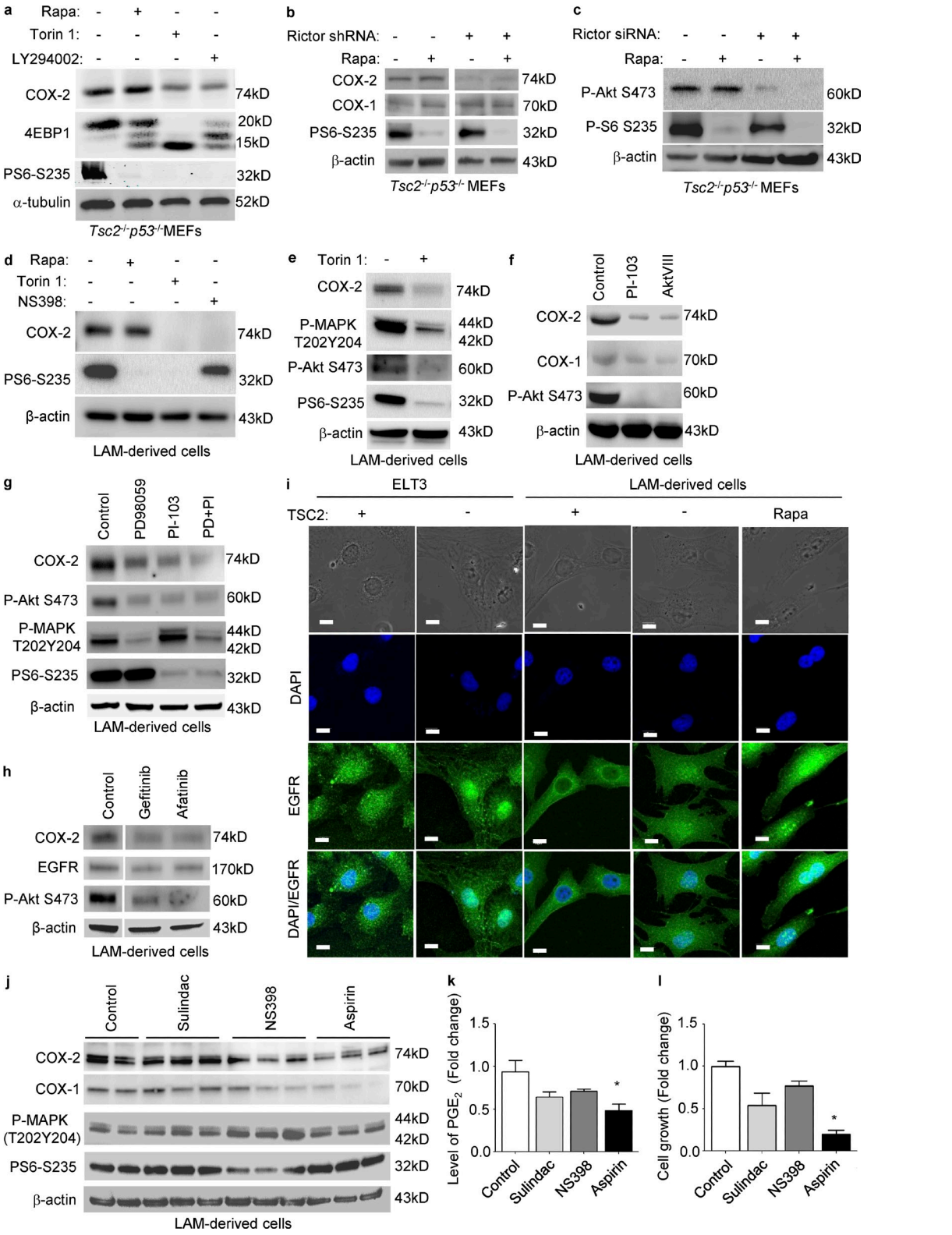

Figure 4. mTORC2 regulates COX-2 expression via PI3K–AKT pathway in TSC2-deficient cells. (a) *Tsc2*$^{-/-}$*p53*$^{-/-}$ MEFs were treated with 20 nM rapamycin, 250 nM Torin 1, or 20 µM LY294002 for 24 h. Levels of COX-2, 4EBP1, and phospho-S6 (S235/236) were assessed by immunoblot. (b and c) *Tsc2*$^{-/-}$*p53*$^{-/-}$ MEFs were transfected with Rictor shRNA or control shRNA, and then selected with puromycin to obtain stable cells. Control shRNA or with Rictor shRNA-*Tsc2*$^{-/-}$*p53*$^{-/-}$ MEFs were treated with vehicle or 20 nM rapamycin for 24 h. Levels of COX-2, COX-1, phospho-S6 (S235/236), and phospho-Akt (S473) were assessed by immunoblot. (d) LAM patient–derived cells (TSC^{-}) cells were treated with 20 nM rapamycin, or 250 nM Torin 1, or

we generated stable knockdown of Rictor, an mTORC2 component, in *Tsc2*$^{-/-}$*p53*$^{-/-}$ MEFs. Rictor silencing profoundly decreased the level of COX-2 and phosphorylation of S6, supporting the notion that mTORC2 is a critical mediator of COX-2 expression in TSC2-deficient cells (Fig. 4 b). Moreover, we found that Rictor knockdown markedly reduced phosphorylation of Akt (S473), a direct target of mTORC2 (Fig. 4 c), indicating the potential impact of mTORC2–Akt axis on COX-2 expression in *Tsc2*$^{-/-}$*p53*$^{-/-}$ MEFs. Why does 4a look so different from 4d? Note that COX-2 is reduced a little with Torin1 in 4a, whereas it's gone in 4d.

To examine the effect of Torin 1 on COX-2 expression in LAM patient–derived cells, we treated 621–101 TSC2^{-} cells with Torin 1 for 24 h. Torin 1 markedly decreased the level of COX-2. However, rapamycin treatment did not affect COX-2 expression in TSC2-deficient 621–101 cells. NS398, a COX-2 inhibitor, strongly decreased the levels of COX-2 in TSC2-deficient cells (Fig. 4 d). Interestingly, Torin 1 treatment decreased phosphorylation of both p44/42–MAPK T202/Y204 and PI3K–Akt S473 (Fig. 4 e). To prove that Akt is a critical mediator of COX-2 expression in LAM patient–derived cells, we treated 621–101 cells with PI-103 (a dual inhibitor of PI3K and mTOR) or Akt-VIII (a selective Akt inhibitor), for 24 h, and found that both inhibitors strongly decreased the levels of COX-2 without affecting COX-1 (Fig. 4 f).

It has been reported that TSC2 does not regulate mTORC2 activation (Dalle Pezze et al., 2012). We have found that mTORC2 is involved in COX-2 expression in TSC2-deficient cells. In another experiments, we found that COX-2 expression was decreased partially by treatment of PD98059 (MEK1/2 inhibitor) or PI-103 (Akt inhibitor), but more strongly by the combination of PD98059 and PI-103 (Fig. 4 g), suggesting that both MEK1/2-MAPK and PI3K–Akt pathways contribute to COX-2 expression. Collectively, our data indicate that mTORC2-Akt plays a critical role in mediating COX-2 expression in TSC2-deficient cells.

To further define the mechanism by which TSC2 acts as a negative regulator of COX-2 protein expression, we focused on epidermal growth factor receptor (EGFR), a known regulator of COX-2 expression and prostaglandin production (Mann et al., 2005; Brand et al., 2013). We found that TSC2-deficient cells treated with the anti-EGFR agents Afatinib and Gefitinib exhibited decreased levels of COX-2 protein, compared with vehicle control (Fig. 4 h). Interestingly, using confocal microscopy, we observed that TSC2 deficiency resulted in abundant nuclear localization of EGFR in comparison with TSC2-addback in two cell types, rat uterine leiomyoma–derived and LAM patient–derived cells (Fig. 4 i). Furthermore, EGFR nuclear localization was not affected by rapamycin treatment (Fig. 4 i), supporting rapamycin-insensitive up-regulation of COX-2 expression and prostaglandin production. Concomitantly, treatment with two PI3K–Akt inhibitors, Akt VIII or PI-103, suppressed COX-2 expression (Fig. 4 f, g). Together, these data support a model in which TSC2 negatively regulates COX-2 expression via effects on nuclear and cytoplasmic localization of EGFR.

Aspirin treatment inhibits the proliferation of TSC2-deficient cell and reduces urinary levels of prostaglandins in vitro

To determine whether inhibition COX-2 impacts the proliferation of TSC2-deficient cells, we treated 621–101 cells with Sulindac (a COX-1 inhibitor), NS398 (a COX-2 inhibitor), or aspirin (an irreversible COX-1 and COX-2 inhibitor that works by blocking enzymatic activities, and also acetylates COX-2, resulting in production of 15-epi-LXA_4, an anti-inflammatory/antitumor compound) for 24 h. NS398 and aspirin reduced COX-2 and COX-1 levels without affecting phosphorylation of p44/42–MAPK or S6 (Fig. 4 j). Aspirin significantly decreased PGE_2 levels (Fig. 4 k) and reduced proliferation of TSC2-deficient 621–101 cells (Fig. 4 l).

Inhibition of COX-2 suppresses renal tumorigenesis and inhibits the progression of xenograft tumor of TSC2-deficient cells in preclinical models

To determine the efficacy of inhibition of COX-2 in vivo, first, we used the COX-2–specific inhibitor Celecoxib to treat *Tsc2*$^{+/-}$ mice, which develop spontaneous renal cystadenomas at age of 4 mo. We found that treatment with Celecoxib strongly suppressed microscopic renal lesions in *Tsc2*$^{+/-}$ mice by ∼50% after 4 mo of treatment (0.1% wt/wt in chow) relative to vehicle control (Fig. 5, a and b). These data indicate that COX-2 is responsible for renal tumorigenesis.

We next assessed the possible benefit of aspirin in a xenograft tumor model of TSC2-deficient ELT3-luciferase-expressing cells. Aspirin treatment for 3 wk decreased the intensity of bioluminescence (Fig. 5, c and d), and decreased the tumor

50 µM NS398 for 24 h. Levels of COX-2 and phospho-S6 (S235/236) were assessed by immunoblot. (e) TSC2-deficient LAM patient–derived cells were treated with 250 nM Torin 1 for 24 h. Levels of COX-2, phospho-p44/42–MAPK, phospho-Akt S473, and phospho-S6 (S235/236) were assessed by immunoblot. (f) TSC2-deficient LAM patient–derived cells were treated with 5 µM PI-103 or 5 µM AKTVIII for 24 h. Levels of COX-2 and phospho-Akt (S473) were assessed by immunoblot. (g) TSC2-deficient LAM patient–derived cells were treated with 50 µM PD98059, 5 µM PI-103, or PD98059 plus PI-103 for 24 h. Levels of COX-2, phospho-Akt S473, phospho-p44/42–MAPK, and phospho-S6 (S235/236) were assessed by immunoblot. (h) TSC2-deficient LAM patient–derived cells were treated with 1 µM Gefitinib or 1 µM Afatinib for 24 h. Levels of COX-2, EGFR, and phospho-Akt S473 were assessed by immunoblot. (i) ELT3 cells expressing empty vector (TSC^{-}) and TSC2-addback (TSC2^{+}), or LAM patient–derived cells (TSC^{-}) cells and TSC2-addback cells (TSC2^{+}) were treated with 20 nM rapamycin (Rapa) for 24 h. Subcellular localization of EGFR was examined using confocal microscopy. Bar, 10 µM. (j) Cells were treated with 50 µM Sulindac, 50 µM NS398, or 450 µM aspirin for 24 h. Levels of COX-1, COX-2, phospho-p44/42 MAPK, and phospho-S6 were assessed by immunoblot. (a–j) Results are representative of two to four different experiments. (k) PGE_2 levels from conditioned media were measured (ELISA). Results are representative of six sets of independent samples per group. (l) Cell proliferation after drug treatment was measured using MTT assay. Results are representative of 12 sets of independent samples per group. *, $P < 0.05$; Student's *t* test.

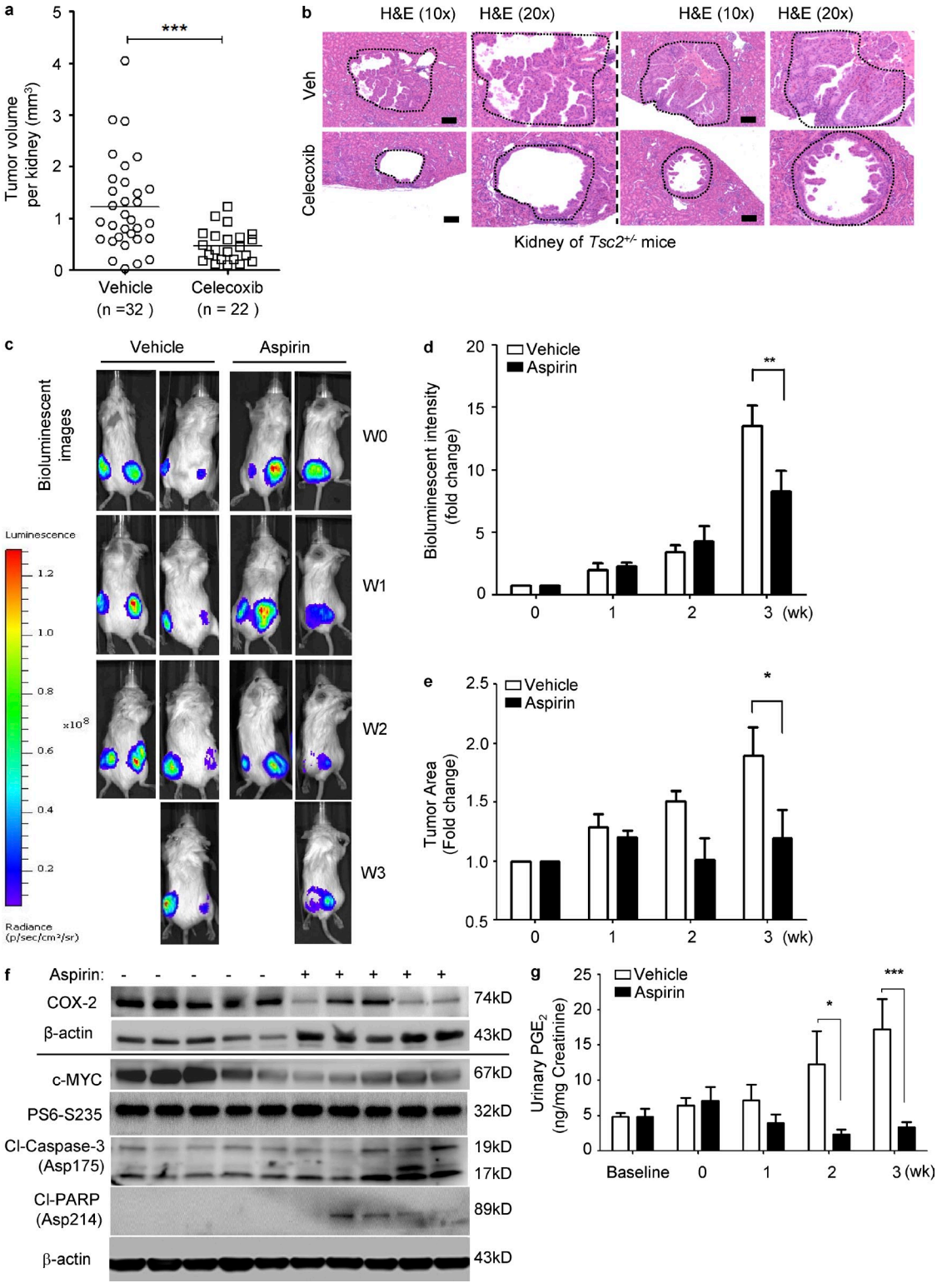

Figure 5. Inhibition of COX-2 suppresses renal tumorigenesis and inhibits the progression of xenograft tumor of TSC2-deficient cells in preclinical models. (a and b) *Tsc2*$^{+/-}$ mice were treated with either vehicle or Celecoxib (0.1% in mouse chow) for one month, and then sacrificed for analysis at the end of treatment. Renal cystadenoma histology and microscopic kidney tumor scores were assessed. (a) Microscopic kidney tumor scores are plotted on a linear scale (P = 0.0002). Data are analyzed from 16 vehicle and 11 Celecoxib treatment groups. (b) Two cystadenomas are shown. Results are representatives of 11 or 16 mice per group. Bar, 100 µM. (c–g) Female CB17-scid mice were inoculated with ELT3-luciferase cells subcutaneously. Mice were treated with either vehicle or aspirin (100 mg/kg/day in the drinking water) for 3 wk (n = 9). Results are representative of five to eight mice per

size (Fig. 5 e). Tumors also had reduced expression of COX-2 and c-Myc, and increased levels of cleaved-caspase-3 and cleaved-PARP (Fig. 5 f). Aspirin-treated mice bearing ELT3 xenograft tumors had markedly reduced urinary levels of PGE_2 (Fig. 5 g), consistent with strong inhibition of each of COX-1 and COX-2, as expected (Fig. 4 j). These data indicate that aspirin reduces PGE_2 production and tumor growth in this TSC2-deficient xenograft model.

Evidence for COX-2 activation in vivo in LAM

We then examined whether these in vitro and xenograft model findings were relevant to human LAM. Accordingly, LAM lungs were found to express higher levels of COX-2 (PTGS2) in comparison with control lungs (Fig. 6 a). Furthermore, immunohistochemistry analyses showed that COX-2 expression was specifically increased in pulmonary LAM nodules (arrows), which also expressed both smooth muscle actin and phospho-S6 (Fig. 6 b). To examine the functional effects of COX-2 expression in LAM, 15-epi-lipoxin A_4 (LXA_4), a product of aspirin-acetylated COX-2, was measured in exhaled breath condensate (EBC) from three LAM subjects (Table 2). LXA_4 was detected in EBCs and the levels were increased with aspirin (Fig. 6 c). LXA_4 decreases proliferation of A549 cells (Human lung adenocarcinoma; Clària et al., 1996) and also reduced the growth of LAM patient–derived 621–101 cells at 100 nM (Fig. 6 d). In a separate experiment, the 15-epi-LXA_4 integrity was confirmed by UV-Vis spectrophotometry to ensure the presence of the diagnostic tetraene chromophore and accurate quantitation and HPLC to ensure that only a single peak was present without evidence for isomerization. (Fig. 6 e). We next performed a dose–response of LXA_4 and found that LXA_4 at 500 nM exhibited the strongest inhibitory effect on cell growth (Fig. 6 e).

Urinary PGE_2 levels were measured in 29 LAM patients and in 18 healthy women; however, these levels were not significantly different between two groups (Fig. 6 f). Because renal prostaglandin production can significantly influence urinary prostaglandin levels, we next measured PGE_2 and 6-keto-$PGF_{1\alpha}$ levels in sera from 14 LAM patients and 13 healthy women. The mean serum PGE_2 level of LAM patients (27.8 ± 1.8 pg/ml) was higher than that of healthy women (19.6 ± 1.4 pg/ml; $P = 0.0021$; Fig. 6 g). In addition, the mean serum 6-keto-PGF1α level of LAM patients (192.2 ± 64.9 pg/ml) was also higher compared with the mean in healthy women (82.6 ± 6.3 pg/ml; $P = 0.0006$; Fig. 6 h).

DISCUSSION

LAM is a neoplastic disorder in which smooth muscle-like cells with biallelic inactivation of *TSC2* leads to hyperactivation of mTORC1. This fundamental mechanistic insight led to the recent reported success in treating LAM patients with rapamycin. However, mTORC1-independent effects of TSC2 loss are also known (Yu and Henske, 2010; Neuman and Henske, 2011). The marked female predominance of LAM suggests that estradiol promotes disease progression. In this study, we identified an estradiol-induced prostaglandin metabolic signature in TSC2-deficient ELT3 cells in vitro and in vivo. Prostaglandins, synthesized via COX-1/COX-2, appear to play important roles in cancer progression (FitzGerald and Patrono, 2001; Müller, 2004; Wang et al., 2007; Wang and Dubois, 2010), although their precise role is still hotly debated. Estradiol-dependent prostaglandin production has been studied in other models. Estradiol activated COX-2 and increased prostacyclin synthesis in mouse aortic smooth muscle cells (Egan et al., 2004). Increased levels of PGE_2 causes enhanced aromatase expression and local estradiol production in breast tissue (Subbaramaiah et al., 2012). However, the relationship between prostaglandins and TSC/LAM has not been investigated previously. Remarkably, we found that estradiol enhances the expression of COX-2 and induces production of PGE_2 in TSC2-deficient cells in vitro and in vivo. Furthermore, we identified a novel function of TSC2 as a negative regulator of COX-2 expression and prostaglandin biosynthesis. Interestingly, this regulation appears to be rapamycin-insensitive but sensitive to Akt inhibition and Rictor knockdown, suggesting that COX-2 may be regulated by Akt in TSC2-deficient cells.

We also demonstrated that COX-2 is abundant in LAM lesions, and that serum levels of PGE_2 are elevated in LAM patients. Collectively, our data suggest that COX-2 may play an important role in LAM pathogenesis.

NS398 and aspirin are direct enzyme inhibitors of COX-2 and/or COX-1. As expected, we have found that cells treated with NS398 or aspirin exhibited reduced levels of PGE_2 (Fig. 4 k), consistent with this inhibition. However, we also found that both NS398 and aspirin decreased the levels of COX-2 protein. Although this was initially surprising to us, multiple experiments confirmed this effect, and our results are in agreement with previous reports that COX-2 protein expression is reduced by classical nonsteroidal antiinflammatory drugs (NSAIDs), including aspirin and NS398 (Takada et al., 2004; Galamb et al., 2010). Therefore, we think that both enzymatic inhibition and reduction in expression of COX-2 occurs in response to NS398 and aspirin treatment. Aspirin, the prototypical NSAID, covalently modifies both COX-1 and COX-2 by acetylation. We demonstrated that aspirin treatment significantly reduced the growth of xenograft tumors of TSC2-deficient ELT3 cells, and led to reduced urinary levels of PGE_2 and 6-keto-PGF1α, which is consistent with

group. (c and d) Bioluminescent imaging was performed weekly. Bioluminescent intensity in xenograft tumors was recorded and quantified weekly. Data are the mean of bioluminescent intensity in tumors from five to eight mice per group. (e) Tumor area was normalized to the baseline before drug administration. Data represent the mean of tumor area from five to eight mice per group. (f) Immunoblot analysis of COX-2, c-Myc, and phospho-S6 in xenograft tumors from mice treated with aspirin or vehicle. Results represent tumors from five mice from each group. (g) Mouse urinary levels of PGE_2 were measured (ELISA). Data represent the mean of PGE_2 levels from five to eight mice per group. *, $P < 0.05$; **, $P < 0.01$; ***, $P < 0.001$; two-way ANOVA test.

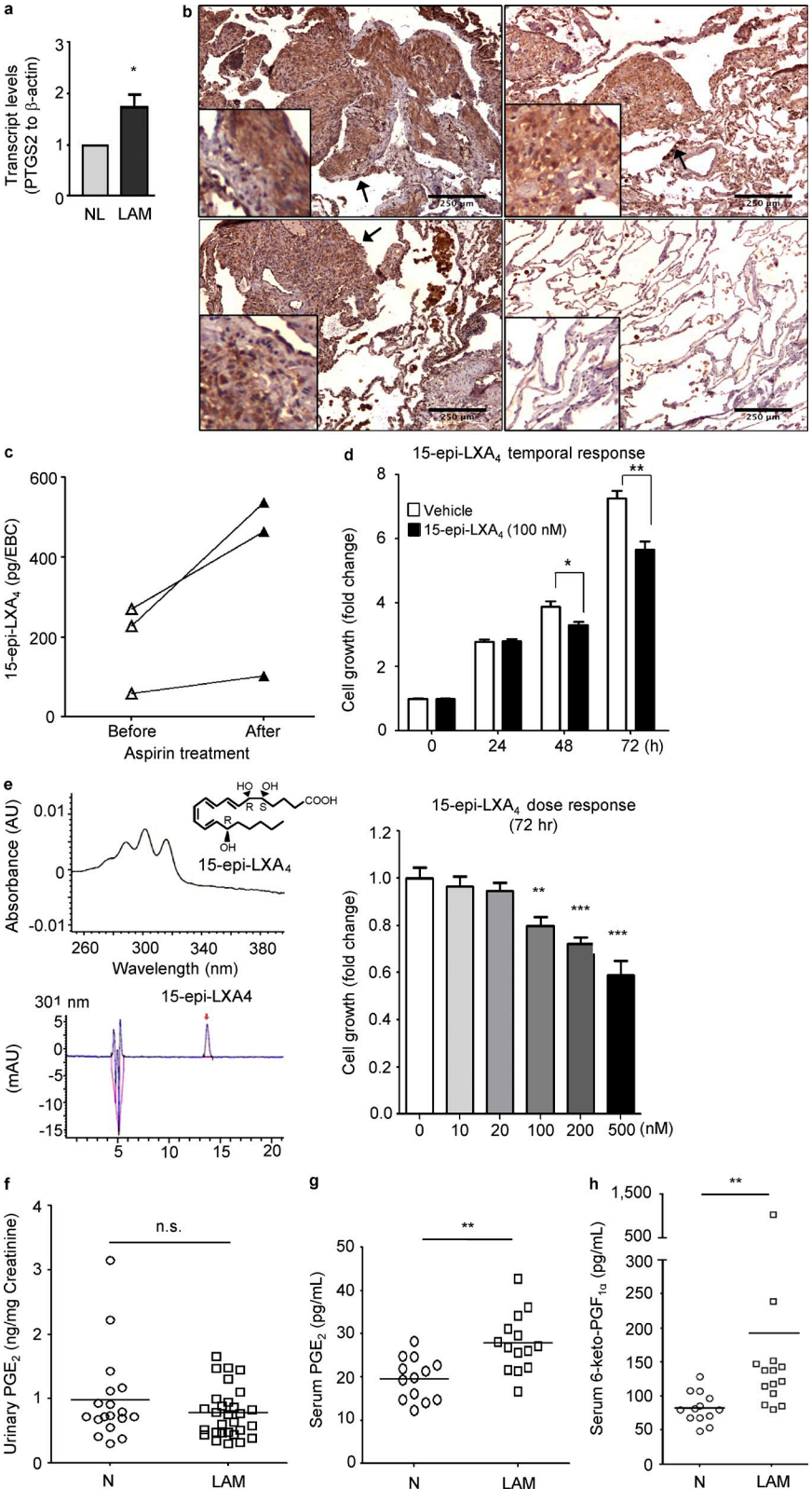

Figure 6. COX-2 expression and prostaglandin production in LAM nodules and LAM patients. (a) Transcript levels of *PTGS2* (COX-2), were measured using real-time RT-PCR on RNA prepared from LAM lung and clinically normal lung samples ($n = 3$ each). Data represent the mean of PTGS2 levels from three subjects from per group. (b) LAM lung tissues stained with COX-2 antibody. Bar, 250 μM. Results are representative of six cases. (c) EBCs were collected from LAM patients before and after aspirin (ASA) treatment (81 mg/day) for 2 wk. Levels of 15-epi-LXA_4 were quantified ($n = 3$). Data represent the mean of 15-epi-LXA4 levels from three subjects from per group. (d) TSC2-deficient LAM patient-derived 621–101 cells were incubated with 100 nM 15-epi-LXA_4 for 0, 24, 48, and 72 h. Cell proliferation was measured using MTT assay. Results are representative of one out of three experiments including twelve sets of samples in each experiment. (e) The 15-epi-LXA4 integrity was confirmed by UV-Vis spectrophotometry to ensure the presence of the diagnostic tetraene chromophore and accurate quantitation and HPLC to ensure that only a single peak was present without evidence for isomerization. TSC2-deficient 621–101 cells were incubated with 10, 20, 100, 200, or 500 nM 15-epi-LXA_4 for 72 h. Cell proliferation was measured using MTT assay. Results are representative of 1 out of 2 experiments, including 16 sample sets in each experiment. (f) Urine samples were collected from LAM patients and healthy women from two geographic locations. Urinary levels of PGE_2 in LAM ($n = 29$) and healthy women (N; $n = 18$) were assessed (ELISA). Serum levels of PGE_2 (g) and 6-keto $PGF_{1\alpha}$ (h) in LAM ($n = 14$) and healthy women (N; $n = 13$) were assessed (ELISA). *, $P < 0.05$; **, $P < 0.01$; ***, $P < 0.001$; Student's *t* test for transcript levels and cell growth tests; Mann Whitney test for prostaglandin quantification in clinical data.

strong inhibition of COX-1/COX-2 function. Furthermore, xenograft tumors from aspirin-treated mice exhibited higher levels of apoptosis compared with vehicle treatment (Fig. 5 f). Although aspirin-acetylated COX-2 inhibits prostaglandin formation, the enzyme is not completely inactivated. Rather, aspirin-acetylated COX-2 catalyzes the conversion of arachidonate

Table 2. Clinical profile of LAM subjects.

	Subject 1	Subject 2	Subject 3
Age	34	47	38
Type of LAM	Sporadic	TSC	Sporadic
Date of Diagnosis	Nov-06	Feb-03	Jan-05
FEV1 (%)	104	70	108
Pneumothorax	No	Yes	No
Pleurodesis procedure	No	Yes	No
Pleural effusion/chylothotax	No	No	No
Hemoptysis	No	No	No

to 15-epi-LXA_4 (Clària et al., 1996). In this manner, aspirin both inhibits prostaglandin production and triggers the formation of 15-epi-LXA_4, a potent inhibitor of malignant cell proliferation (Clària et al., 1996). 15-epi-LXA_4 was present in EBCs from LAM patients, and was increased with oral aspirin ingestion. 15-epi-LXA_4 also decreased LAM-patient–derived cell proliferation (Fig. 6, d and e) Together, these findings suggest that aspirin may have rapamycin-independent beneficial effects in LAM.

LAM is often a progressive disease which leads to respiratory failure and death in the absence of lung transplantation. The recent demonstration that rapamycin has clinical benefit in LAM is a major success. However, not all patients respond to rapamycin, and upon rapamycin withdrawal, lung function decline resumes (McCormack et al., 2012). Hence, lifelong treatment of LAM patients with rapamycin may be required to maintain benefit, with unknown long-term toxicities. Our findings suggest that aspirin and/or other COX-1/COX-2 inhibitors may have significant benefit in slowing LAM progression. The well-known side-effect and toxicity profile of these drugs make them attractive candidates for long-term therapy in LAM patients. It is also possible that other neoplastic conditions associated with mTOR hyperactivation could be responsive to these agents. Further preclinical and clinical investigation is warranted to explore these possibilities.

MATERIALS AND METHODS

Cell culture and reagents. ELT3 cells (Eker rat uterine leiomyoma-derived cells; Howe et al., 1995a,b) and LAM patient–derived 621–101, 621–102, and 621–103 cells were cultured in IIA complete medium. *Tsc2*$^{-/-}$*p53*$^{-/-}$ MEFs, HEK293, HeLa, U2OS, and OVARC5 cells were cultured in DMEM supplemented with 10% FBS. 17-β-estradiol (10 nM; Sigma-Aldrich), rapamycin (20 nM; Biomol), Torin 1 (250 nM; Tocris), LY294002 (20 μM; Cell Signaling Technology), NS398 (50 μM; Cayman Chemical), Sulindac (50 μM; Cayman Chemical), aspirin (450 μM; Sigma-Aldrich), Celecoxib (Novartis), PI-103 (5 μM;Tocris), and AktVIII (5 μM; Millipore), and Wortmannin (1 μM; Cell Signaling Technology) were used as indicated. 15-epi-LXA_4 (10–500 nM) was obtained from Millipore. The integrity of 15-epi-LXA_4 was determined by UV-Vis spectrometry and HPLC. Because of the volatile nature of this product, stock solutions were stored at −80°C.

Animal studies. All animal work was performed in accordance with protocols approved by the IACUC-CHB. For xenograft tumor establishment, 2×10^6 ELT3-luciferase cells were inoculated bilaterally into the posterior back region of female intact CB17-SCID mice (Taconic) as previously described (Yu et al., 2009; Parkhitko et al., 2011; Liu et al., 2012). 5 wk after cell inoculation, mice bearing subcutaneous tumors were randomized into two groups: vehicle control ($n = 5$) and aspirin ($n = 5$; 100 mg/kg/day, in drinking water). Tumor area (width × length) was measured weekly using calipers. Urine specimens were collected from mice for PGE_2 and 6-keto-$PGF1_\alpha$ measurement. For spontaneously arising renal tumor model, *Tsc2*$^{+/-}$ mice, originally generated in this laboratory (Onda et al., 1999), were serially crossed with A/J mice for over five generations. These pure strain mice were used in all experiments. Celecoxib (Novartis) was administered by mouse chow (0.1%) for 4 mo, beginning at 1 mo of age, and then sacrificed for renal tumor assessment at the end of treatment (5 mo).

Microscopic kidney tumor scores. Mouse kidneys were removed rapidly after euthanasia and fixed overnight in 10% formalin. Kidneys were then prepared for histological evaluation in stereotypical fashion by cutting the kidney into sections at 1-mm sections.

Microscopic kidney tumor scores were determined in a semiquantitative fashion by a single blinded observer. The set of 1-mm sections were prepared as H&E-stained 8-μm sections. Each tumor or cyst identified was measured to determine its length and width in two dimensions, as well as the percentage of the lumen filled by tumor (this was 0% for a simple cyst, and 100% for a completely filled, solid adenoma). These measurements were converted into a measurement of tumor volume per lesion using the following formula: tumor volume = maximum (tumor percent, 5)/100 × 3.14159/6 × 1.64 × (tumor length × tumor width) **1.5 (Auricchio et al., 2012). The total tumor volume per kidney was then equal to sum of the tumor volume of each lesion identified. Comparisons between sets of mice for tumor measurements were made using the nonparametric Mann-Whitney test in Prism (GraphPad Software, Inc.).

Bioluminescent reporter imaging. 10 min before imaging, animals were injected with luciferin (120 mg/kg; i.p.; Xenogen). Bioluminescent signals were recorded using the Xenogen IVIS System. Total photon flux of tumors was analyzed as previously described (Yu et al., 2009).

Confocal microscopy. ELT3 cells and LAM-derived cells were plated on glass coverslips in 12-well tissue culture plates overnight. Cells were serum starved overnight, and then treated with 20 nM rapamycin for 24 h. Cells were rinsed with PBS twice, fixed with warm 4% paraformaldehyde, permeabilized with 0.2% Triton X-100, blocked in 3% BSA/PBS for 1 h, incubated with primary antibody 1% BSA in PBS for 1 h at room temperature, and then incubated with secondary antibodies for 1 h. Images were captured with a FluoView FV-10i Olympus Laser Point Scanning Confocal Microscope.

Expression array analysis. Re-analysis of previously published expression array data (GEO accession no. GSE16944; Lee et al., 2010) was performed using the online tool GEO2R. Transcript levels of *PTGS2* (COX-2; ID: 238018) and *PTGIS* (prostacyclin synthase; ID: 454010) were compared between TSC2-deficient and TSC2-addback ($TSC2^+$) cells, or rapamycin- and vehicle-treated TSC2-deficient cells.

Quantitative RT-PCR. RNA from cultured cells and xenograft tumors was isolated using RNeasy Mini kit (QIAGEN). Gene expression was quantified using One-Step qRT-PCR kits (Invitrogen) in the Applied Biosystems Step One Plus Real-Time PCR System and normalized to β-actin.

Immunoblotting and antibodies. Cells were lysed in m-PER buffer (Thermo Fisher Scientific). The following antibodies were used: COX-1, COX-2, EGFR, phospho-p44/42–MAPK (T202/Y204), phospho-S6 (S235/236), phospho-Akt (S473), cleaved caspase 3, and cleaved PARP (Cell Signaling Technology); tuberin and c-Myc (Santa Cruz Biotechnology, Inc.); smooth muscle actin (BioGenex); β-actin (Sigma-Aldrich); and Alexa Fluor 488 goat anti–rabbit IgG (H+L) antibody (Invitrogen).

Metabolomic profiling. 100 µg of frozen biopsy tissue was submitted to Metabolon, Inc. for sample extraction and analysis. In brief, Metabolon performed cold methanol extraction of mechanically disaggregated tissue samples and these extracts were split into three aliquots. The reproducibility of the extraction protocol was assessed by the recovery of xenobiotic compounds spiked into every tissue sample before extraction. These aliquots were processed and characterized by one of the three analytical methods previously described (Evans et al., 2009): UHPLC-ESI-MS/MS in the positive ion mode, UHPLC-ESI-MS/MS in the negative ion mode, and sialylation followed by GC-EI-MS. Chromatographic timelines were standardized using a series of xenobiotics that elute at specified intervals throughout each chromatographic run. The technical variability of each analytical platform was assessed by repeated characterization of a pooled standard that contained an aliquot of each sample within the study. Metabolon's global screening platform utilizes a nontargeted approach (Evans et al., 2009). For LC-MS/MS, after peak identification and quality control filtering (signal greater than 3x background, retention index within a prespecified platform-dependent window, quant ions to library match within 0.4 m/z, and the MS/MS forward and reverse scores), the metabolites' relative concentrations were obtained from median-scaled day-block normalized data for each compound. In vitro data were normalized to total protein levels as measured by Bradford assay. Eicosanoids identified by the Metabolon platform in this study were measured by LC-MS/MS run in the negative mode. Fragmentation of the molecule's quant ion generated a pattern of ions that matched in mass and relative intensities to a purified standard as described by DeHaven et al. (2010). In this study, the data were derived using a nontargeted method that does not incorporate labeled standards. However, in cases where targeted methods have been created and used to validate Metabolon screening platform, the results from the screening platform have shown a high degree of correlation with the targeted/absolute quantification methods and clinical measurements, when available (Sreekumar et al., 2009; Zhang et al., 2011).

Cell viability assay. Cell viability was determined by MTT assay (Sigma-Aldrich).

Short hairpin RNA (shRNA) down-regulation. 293T packaging cells were transfected with Rictor shRNA or non-targeting shRNA vectors using Mirus Trans-IT TKO Transfection reagent (Mirus). *Tsc2*$^{-/-}$*p53*$^{-/-}$ MEFs were infected with lentivirus containing Rictor shRNA, or non-Targeting shRNA. Cells were harvested 48 h after transfection and then selected against puromycin. Stable clones were harvested for future experiments.

Immunohistochemistry. Sections were deparaffinized, incubated with primary antibodies and biotinylated secondary antibodies, and counterstained with Gill's Hematoxylin.

Quantification of prostaglandin levels. Levels of PGEM (a stable metabolite of PGE_2), 6-keto-$PGF_{1\alpha}$ (a stable metabolite of prostacyclin), and creatinine were measured using ELISA kits (Cayman Chemical). Levels of secreted prostaglandins were normalized to vehicle control and expressed as fold change. Urinary levels of prostaglandins were normalized to creatinine levels and expressed as nanograms per milliliter.

Statistical analyses. Statistical analyses were performed using Student's *t* test when comparing two groups for in vitro and in vivo studies. Welch's *t* tests and Wilcoxon rank sum tests were performed for metabolomic profiling. Two-way ANOVA test was performed in xenograft tumor-aspirin studies. Mann-Whitney tests were used for prostaglandin quantification in clinical data.

We are grateful for Dr. C Walker (Texas A&M Health Science Center) for providing ELT3 cells, Ms. E. Peters (The Center for LAM Research and Clinical Care - Brigham and Women's Hospital) for human specimen acquisition, Mr. B. Ith, and Dr. M Perrella for specimen preparation, Dr. C. Jiang (Peking Union Medical College, China) for providing access to research facility, and Dr. I. Rosas for providing non-LAM lung tissues. We thank Dr. A. Choi for valuable discussion and critical review of the manuscript. We gratefully acknowledge LAM patients and healthy volunteers for their valuable contribution to this study.

A. Csibi and X. Gu are LAM Foundation postdoctoral fellows. J. Li is a Tuberous Sclerosis Alliance postdoctoral fellow. J. Blenis is a LAM Foundation established investigator. This study is supported by The LAM Foundation, The Adler Foundation, The LAM Treatment Alliance (to E.P. Henske)., National Institutes of Health Grant GM51405 (to J. Blenis), the National Heart Lung and Blood Institute grants HL68669 (to B.D. Levy) and HL118760 (to E.P. Henske), the National Cancer Institute grants 1P01CA120964 (to D. Kwiatkowski) and HL098216 (to J.J. Yu), the Department of Defense Exploratory Idea Development Award (W81XWH-12-1-0442 to J.J. Yu), and Biomedical Research Institute-BWH Microgrants to C. Li and J.J. Yu.

B.D. Levy is an inventor on patents on lipoxins assigned to Brigham and Women's Hospital, some of which are licensed for clinical development. The interests of B.D. Levy were reviewed and are managed by the Brigham and Women's Hospital and Partners HealthCare in accordance with their conflict of interest policies. The other authors have no conflicting financial interests.

Submitted: 24 May 2013
Accepted: 9 December 2013

REFERENCES

Astrinidis, A., L. Khare, T. Carsillo, T. Smolarek, K.S. Au, H. Northrup, and E.P. Henske. 2000. Mutational analysis of the tuberous sclerosis gene TSC2 in patients with pulmonary lymphangioleiomyomatosis. *J. Med. Genet.* 37:55–57. http://dx.doi.org/10.1136/jmg.37.1.55

Auricchio, N., I. Malinowska, R. Shaw, B.D. Manning, and D.J. Kwiatkowski. 2012. Therapeutic trial of metformin and bortezomib in a mouse model of tuberous sclerosis complex (TSC). *PLoS ONE.* 7:e31900. http://dx.doi.org/10.1371/journal.pone.0031900

Brand, T.M., M. Iida, N. Luthar, M.M. Starr, E.J. Huppert, and D.L. Wheeler. 2013. Nuclear EGFR as a molecular target in cancer. *Radiother. Oncol.* 108:370–377.

Clària, J., M.H. Lee, and C.N. Serhan. 1996. Aspirin-triggered lipoxins (15-epi-LX) are generated by the human lung adenocarcinoma cell line (A549)-neutrophil interactions and are potent inhibitors of cell proliferation. *Mol. Med.* 2:583–596.

Costello, L.C., T.E. Hartman, and J.H. Ryu. 2000. High frequency of pulmonary lymphangioleiomyomatosis in women with tuberous sclerosis complex. *Mayo Clin. Proc.* 75:591–594. http://dx.doi.org/10.4065/75.6.591

Crino, P.B., K.L. Nathanson, and E.P. Henske. 2006. The tuberous sclerosis complex. *N. Engl. J. Med.* 355:1345–1356. http://dx.doi.org/10.1056/NEJMra055323

Dabora, S.L., S. Jozwiak, D.N. Franz, P.S. Roberts, A. Nieto, J. Chung, Y.S. Choy, M.P. Reeve, E. Thiele, J.C. Egelhoff, et al. 2001. Mutational analysis in a cohort of 224 tuberous sclerosis patients indicates increased severity of TSC2, compared with TSC1, disease in multiple organs. *Am. J. Hum. Genet.* 68:64–80. http://dx.doi.org/10.1086/316951

Dalle Pezze P., A.G. Sonntag, A. Thien, M.T. Prentzell, M. Gödel, S. Fischer, et al. 2012. A dynamic network model of mTOR signaling reveals TSC-independent mTORC2 regulation. *Sci. Signal.* 5:ra25.

Dehaven, C.D., A.M. Evans, H. Dai, and K.A. Lawton. 2010. Organization of GC/MS and LC/MS metabolomics data into chemical libraries. *J. Cheminform.* 2:9.

Düvel, K., J.L. Yecies, S. Menon, P. Raman, A.I. Lipovsky, A.L. Souza, E. Triantafellow, Q. Ma, R. Gorski, S. Cleaver, et al. 2010. Activation of a metabolic gene regulatory network downstream of mTOR complex 1. *Mol. Cell*. 39:171–183. http://dx.doi.org/10.1016/j.molcel.2010.06.022

Egan, K.M., J.A. Lawson, S. Fries, B. Koller, D.J. Rader, E.M. Smyth, and G.A. Fitzgerald. 2004. COX-2-derived prostacyclin confers atheroprotection on female mice. *Science*. 306:1954–1957. http://dx.doi.org/10.1126/science.1103333

Evans, A.M., C.D. DeHaven, T. Barrett, M. Mitchell, and E. Milgram. 2009. Integrated, nontargeted ultrahigh performance liquid chromatography/electrospray ionization tandem mass spectrometry platform for the identification and relative quantification of the small-molecule complement of biological systems. *Anal. Chem*. 81:6656–6667.

FitzGerald, G.A., and C. Patrono. 2001. The coxibs, selective inhibitors of cyclooxygenase-2. *N. Engl. J. Med*. 345:433–442. http://dx.doi.org/10.1056/NEJM200108093450607

Galamb, O., S. Spisák, F. Sipos, K. Tóth, N. Solymosi, B. Wichmann, T. Krenács, G. Valcz, Z. Tulassay, and B. Molnár. 2010. Reversal of gene expression changes in the colorectal normal-adenoma pathway by NS398 selective COX2 inhibitor. *Br. J. Cancer*. 102:765–773. http://dx.doi.org/10.1038/sj.bjc.6605515

Henske, E.P., and F.X. McCormack. 2012. Lymphangioleiomyomatosis - a wolf in sheep's clothing. *J. Clin. Invest*. 122:3807–3816. http://dx.doi.org/10.1172/JCI58709

Howe, S.R., M.M. Gottardis, J.I. Everitt, T.L. Goldsworthy, D.C. Wolf, and C. Walker. 1995a. Rodent model of reproductive tract leiomyomata. Establishment and characterization of tumor-derived cell lines. *Am. J. Pathol*. 146:1568–1579.

Howe, S.R., M.M. Gottardis, J.I. Everitt, and C. Walker. 1995b. Estrogen stimulation and tamoxifen inhibition of leiomyoma cell growth in vitro and in vivo. *Endocrinology*. 136:4996–5003. http://dx.doi.org/10.1210/en.136.11.4996

Jaeschke, A., J. Hartkamp, M. Saitoh, W. Roworth, T. Nobukuni, A. Hodges, J. Sampson, G. Thomas, and R. Lamb. 2002. Tuberous sclerosis complex tumor suppressor-mediated S6 kinase inhibition by phosphatidylinositide-3-OH kinase is mTOR independent. *J. Cell Biol*. 159:217–224. http://dx.doi.org/10.1083/jcb.jcb.200206108

Karbowniczek, M., A. Astrinidis, B.R. Balsara, J.R. Testa, J.H. Lium, T.V. Colby, F.X. McCormack, and E.P. Henske. 2003. Recurrent lymphangiomyomatosis after transplantation: genetic analyses reveal a metastatic mechanism. *Am. J. Respir. Crit. Care Med*. 167:976–982. http://dx.doi.org/10.1164/rccm.200208-969OC

Krymskaya, V.P. 2012. Treatment option(s) for pulmonary lymphangioleiomyomatosis: progress and current challenges. *Am. J. Respir. Cell Mol. Biol*. 46:563–565. http://dx.doi.org/10.1165/rcmb.2011-0381ED

Lee, P.S., S.W. Tsang, M.A. Moses, Z. Trayes-Gibson, L.L. Hsiao, R. Jensen, R. Squillace, and D.J. Kwiatkowski. 2010. Rapamycin-insensitive up-regulation of MMP2 and other genes in tuberous sclerosis complex 2-deficient lymphangioleiomyomatosis-like cells. *Am. J. Respir. Cell Mol. Biol*. 42:227–234. http://dx.doi.org/10.1165/rcmb.2009-0050OC

Liu, F., E.P. Lunsford, J. Tong, Y. Ashitate, S.L. Gibbs, J. Yu, H.S. Choi, E.P. Henske, and J.V. Frangioni. 2012. Real-time monitoring of tumorigenesis, dissemination, & drug response in a preclinical model of lymphangioleiomyomatosis/tuberous sclerosis complex. *PLoS ONE*. 7:e38589. http://dx.doi.org/10.1371/journal.pone.0038589

Mann, J.R., M.G. Backlund, and R.N. DuBois. 2005. Mechanisms of disease: Inflammatory mediators and cancer prevention. *Nat. Clin. Pract. Oncol*. 2:202–210.

Manning, B.D. 2010. The role of target of rapamycin signaling in tuberous sclerosis complex. In Tuberous Sclerosis Complex. V.H. Whittlemore, D.J. Kwiatkowski, and E.A. Thiele, editors. Wiley-VCH, Weinheim, Germany. Pages 87-115. http://dx.doi.org/10.1002/9783527630073.ch6

McCormack, F.X., R.J. Panos, and B.C. Trapnell, editors. 2010. Molecular Basis of Pulmonary Disease Insights from Rare Lung Disorders. Human Press, New York. http://dx.doi.org/10.1007/978-1-59745-384-4

McCormack, F.X., Y. Inoue, J. Moss, L.G. Singer, C. Strange, K. Nakata, A.F. Barker, J.T. Chapman, M.L. Brantly, J.M. Stocks, et al. MILES Trial Group. 2011. Efficacy and safety of sirolimus in lymphangioleiomyomatosis. *N. Engl. J. Med*. 364:1595–1606. http://dx.doi.org/10.1056/NEJMoa1100391

McCormack, F.X., W.D. Travis, T.V. Colby, E.P. Henske, and J. Moss. 2012. Lymphangioleiomyomatosis: calling it what it is: a low-grade, destructive, metastasizing neoplasm. *Am. J. Respir. Crit. Care Med*. 186:1210–1212. http://dx.doi.org/10.1164/rccm.201205-0848OE

Müller, R. 2004. Crosstalk of oncogenic and prostanoid signaling pathways. *J. Cancer Res. Clin. Oncol*. 130:429–444.

Neuman, N.A., and E.P. Henske. 2011. Non-canonical functions of the tuberous sclerosis complex-Rheb signalling axis. *EMBO Mol Med*. 3:189–200. http://dx.doi.org/10.1002/emmm.201100131

Onda, H., A. Lueck, P.W. Marks, H.B. Warren, and D.J. Kwiatkowski. 1999. Tsc2(+/-) mice develop tumors in multiple sites that express gelsolin and are influenced by genetic background. *J. Clin. Invest*. 104:687–695. http://dx.doi.org/10.1172/JCI7319

Parkhitko, A., F. Myachina, T.A. Morrison, K.M. Hindi, N. Auricchio, M. Karbowniczek, J.J. Wu, T. Finkel, D.J. Kwiatkowski, J.J. Yu, and E.P. Henske. 2011. Tumorigenesis in tuberous sclerosis complex is autophagy and p62/sequestosome 1 (SQSTM1)-dependent. *Proc. Natl. Acad. Sci. USA*. 108:12455–12460. http://dx.doi.org/10.1073/pnas.1104361108

Plank, T.L., R.S. Yeung, and E.P. Henske. 1998. Hamartin, the product of the tuberous sclerosis 1 (TSC1) gene, interacts with tuberin and appears to be localized to cytoplasmic vesicles. *Cancer Res*. 58:4766–4770.

Ryu, J.H., T.E. Hartman, V.E. Torres, and P.A. Decker. 2012. Frequency of undiagnosed cystic lung disease in patients with sporadic renal angiomyolipomas. *Chest*. 141:163–168. http://dx.doi.org/10.1378/chest.11-0669

Sevigny, M.B., C.F. Li, M. Alas, and M. Hughes-Fulford. 2006. Glycosylation regulates turnover of cyclooxygenase-2. *FEBS Lett*. 580:6533–6536. http://dx.doi.org/10.1016/j.febslet.2006.10.073

Sreekumar, A., L.M. Poisson, T.M. Rajendiran, A.P. Khan, Q. Cao, J. Yu, et al. 2009. Metabolomic profiles delineate potential role for sarcosine in prostate cancer progression. *Nature*. 457:910–914.

Strizheva, G.D., T. Carsillo, W.D. Kruger, E.J. Sullivan, J.H. Ryu, and E.P. Henske. 2001. The spectrum of mutations in TSC1 and TSC2 in women with tuberous sclerosis and lymphangiomyomatosis. *Am. J. Respir. Crit. Care Med*. 163:253–258. http://dx.doi.org/10.1164/ajrccm.163.1.2005004

Subbaramaiah, K., P.G. Morris, X.K. Zhou, M. Morrow, B. Du, D. Giri, L. Kopelovich, C.A. Hudis, and A.J. Dannenberg. 2012. Increased levels of COX-2 and prostaglandin E2 contribute to elevated aromatase expression in inflamed breast tissue of obese women. *Cancer Discov*. 2:356–365. http://dx.doi.org/10.1158/2159-8290.CD-11-0241

Takada, Y., A. Bhardwaj, P. Potdar, and B.B. Aggarwal. 2004. Nonsteroidal anti-inflammatory agents differ in their ability to suppress NF-kappaB activation, inhibition of expression of cyclooxygenase-2 and cyclin D1, and abrogation of tumor cell proliferation. *Oncogene*. 23:9247–9258.

Taveira-DaSilva, A.M., G. Pacheco-Rodriguez, and J. Moss. 2010. The natural history of lymphangioleiomyomatosis: markers of severity, rate of progression and prognosis. *Lymphat. Res. Biol*. 8:9–19. http://dx.doi.org/10.1089/lrb.2009.0024

Wang, D., and R.N. Dubois. 2010. Eicosanoids and cancer. *Nat. Rev. Cancer*. 10:181–193. http://dx.doi.org/10.1038/nrc2809

Wang, M.T., K.V. Honn, and D. Nie. 2007. Cyclooxygenases, prostanoids, and tumor progression. *Cancer Metastasis Rev*. 26:525–534. http://dx.doi.org/10.1007/s10555-007-9096-5

Yu, J., and E.P. Henske. 2010. Dysregulation of TOR signaling in tuberous sclerosis and lymphangioleiomyomatosis. *In* The Enzyme. Academic Press, Burlington. 303-327. http://dx.doi.org/10.1016/S1874-6047(10)27016-6

Yu, J., A. Astrinidis, S. Howard, and E.P. Henske. 2004. Estradiol and tamoxifen stimulate LAM-associated angiomyolipoma cell growth and activate both genomic and nongenomic signaling pathways. *Am. J. Physiol. Lung Cell. Mol. Physiol*. 286:L694–L700. http://dx.doi.org/10.1152/ajplung.00204.2003

Yu, J.J., V.A. Robb, T.A. Morrison, E.A. Ariazi, M. Karbowniczek, A. Astrinidis, C. Wang, L. Hernandez-Cuebas, L.F. Seeholzer, E. Nicolas, et al. 2009. Estrogen promotes the survival and pulmonary metastasis of tuberin-null cells. *Proc. Natl. Acad. Sci. USA*. 106:2635–2640. http://dx.doi.org/10.1073/pnas.0810790106

Zhang, Y., Y. Dai, J. Wen, W. Zhang, A. Grenz, H. Sun, et al. 2011. Detrimental effects of adenosine signaling in sickle cell disease. *Nat. Med*. 17:79–86.